Top-down signaling dynamically mediates information processing in biologically inspired RNNs

Tomas Gallo Aquino[1 *], Robert Kim [2 *], Nuttida Rungratsameetaweemana[1]

[1] Department of Biomedical Engineering, Columbia University, New York, NY 10027, USA

[2] Department of Neurology, Cedars-Sinai Medical Center, Los Angeles, CA 90048, USA

[*] Equal contribution

Correspondence: nr2869@columbia.edu (N.R.)

Abstract

Recent studies have proposed employing biologically plausible recurrent neural networks (RNNs) to explore flexible decision making processes in the brain. However, the mechanisms underlying the integration of bottom-up factors (such as incoming sensory signals) and top-down factors (such as task instructions and selective attention) remain poorly understood, both within the context of these models and the brain. To address this question, we trained biologically inspired RNNs on complex cognitive tasks that require adaptive integration of these factors. By performing extensive dynamical systems analyses, we show that our RNN model is capable of seamlessly incorporating top-down signals with sensory signals to perform the complex tasks. Furthermore, through comprehensive local connectivity analyses, we identified important inhibitory feedback signals that efficiently modulate the bottom-up sensory coding in a task-driven manner. Finally, we introduced an anatomical constraint where a specific subgroup of neurons receives the sensory input signal, effectively creating a designated sensory area within the RNN. Through this constraint, we show that these "sensory" neurons possess the remarkable ability to multiplex and dynamically combine both bottom-up and top-down information. These findings are consistent with recent experimental results highlighting that such integration is a key factor in facilitating flexible decision making. Overall, our work provides a framework for generating testable hypotheses for the hierarchical encoding of task-relevant information.

Introduction

Models based on recurrent neural networks (RNNs) of continuous-variable firing rate units have been widely used to reproduce previously observed experimental findings and to explore neural dynamics associated with cognitive functions such as attention and working memory [1–4]. However, these modeling studies primarily focus on tasks with fixed task and context, thereby forcing the model to predominantly rely on bottom-up processing (i.e., encoding sensory stimuli).

Such an approach does not fully capture the dynamics of the natural environment, where informative top-down information is consistently available and plays a critical role in optimizing the translation of incoming sensory signals into appropriate motor responses. In the real world, there is an abundance of contextual cues, task instructions, and prior knowledge that guide and shape our perception and decision-making processes. Neglecting to take these important top-down factors into models limits our understanding of how neural systems combine bottom-up and top-down information to generate optimal behavior.

To address this knowledge gap, we carefully designed cognitive tasks that require seamless integration of bottom-up sensory inputs with top-down factors. By training biologically inspired RNNs on these tasks and studying the trained networks, we show that disinhibitory circuitry governed by inhibitory-to-inhibitory connections are critical for the intricate interplay between the two essential components of cognitive processing. More specifically, our contributions in this paper are:

1. We develop a biologically plausible RNN model with important biological properties including heterogeneous neuronal timescales, uniform neurotransmitter release characteristics within individual neurons, and sensory input constraints.

2. We introduce a set of complex decision-making tasks that mimic empirical neuroscience studies, featuring: a) orthogonal manipulation of bottom-up and top-down signals and b) diverse top-down signaling with varying temporal dynamics.

3. Our results unveil mechanistic insights into the integration of top-down and bottom-up signals during information processing in a biological context.

4. We present a comprehensive theoretical framework delineating the computational principles employed by our RNN model to flexibly harness distinct top-down signals to guide the analysis of sensory input, thereby optimizing task performance.

Biologically plausible recurrent neural network (RNN) model

In this study, we employed the following continuous-variable recurrent neural network (RNN) model:

$$\boldsymbol{\tau}\frac{d\boldsymbol{x}}{dt} = -\boldsymbol{x}(t) + \boldsymbol{w}\boldsymbol{r}(t) + \boldsymbol{w}_{in}\boldsymbol{u}(t) \tag{1}$$

$$\boldsymbol{r}(t) = \sigma(\boldsymbol{x}(t)) = \frac{1}{1+\exp(-\boldsymbol{x}(t))} \tag{2}$$

$$\boldsymbol{o}(t) = \boldsymbol{w}_{out}\boldsymbol{r}(t) + b \tag{3}$$

where $\boldsymbol{\tau} \in \mathbb{R}^{1\times N}$ refers to the synaptic time constants, $\boldsymbol{x} \in \mathbb{R}^{N\times T}$ denotes the synaptic current variable from from N units across T time-points. By applying a sigmoid nonlinearity, we estimated the firing rates $\boldsymbol{r} \in \mathbb{R}^{N\times T}$ based on the synaptic current values ($\boldsymbol{x}$). The connection weights from the time-varying inputs ($\boldsymbol{u} \in \mathbb{R}^{N_{in}\times T}$; N_{in}, the number of stimuli) to the network were represented by the weight matrix $\boldsymbol{w}_{in} \in \mathbb{R}^{N\times N_{in}}$. Additionally, $\boldsymbol{w} \in \mathbb{R}^{N\times N}$ contains connection weights between the N units. To compute the network output ($\boldsymbol{o} \in \mathbb{R}^{1\times T}$), we linearly combined all the firing rates specified by the output connection weight matrix, $\boldsymbol{w}_{out} \in \mathbb{R}^{1\times N}$, along with the constant bias term, b. The network size (N) was set to 1000, and the input signals were given to all the units except for the RNNs used in **Hierarchical organization of inhibitory-to-inhibitory feedback connections** where only the first 200 units received the input.

The dynamics were discretized using the first-order Euler approximation method and using the step size (Δt) of 5 ms:

$$\boldsymbol{x}_t = \left(1 - \frac{\Delta t}{\boldsymbol{\tau}}\right)\boldsymbol{x}_{t-1} + \frac{\Delta t}{\boldsymbol{\tau}}(\boldsymbol{w}\boldsymbol{r}_{t-1} + \boldsymbol{w}_{in}\boldsymbol{u}_{t-1}) \tag{4}$$

where $\boldsymbol{x}_t = \boldsymbol{x}(t)$. Given that the units in this network model communicate through differentiable and continuous signals, a gradient-descent supervised method, known as backpropagation through time (BPTT; [5]), was employed to train our RNNs to perform cognitive tasks. Specifically, the trainable parameters of the model included $\boldsymbol{w}$, $\boldsymbol{\tau}$, $\boldsymbol{w}_{out}$, and b. We used Adam (adaptive moment estimation) optimization algorithm to update these parameters. The learning rate was set to 0.01, and the TensorFlow default values were used for the rest of the parameters including the first and second moment decay rates. To further impose biological constraints, we enforced Dale's law (uniform neurotransmitter release characteristics within separate excitatory and inhibitory neurons) using methods similar to those implemented in previous studies ([2, 6, 7]). To adhere to empirical findings regarding the ratio of excitatory and inhibitory neurons observed in the brain, each RNN consists of 80% excitatory and 20% inhibitory units (i.e., E-I ratio of 80/20; [8–10]).

Importantly, instead of fixing the synaptic decay constant ($\boldsymbol{\tau}$) to a fixed value for all the units, we optimized the parameter for each unit. The parameter was trained to range from 20 ms to 125 ms to model heterogeneous synaptic dynamics of different receptors in the cortex [11, 12]. We initialized the synaptic decay time constant parameter ($\boldsymbol{\tau}$) using

$$\boldsymbol{\tau} = \sigma(\mathcal{N}(0,1))\tau_{step} + \tau_{min}$$

where $\sigma(\cdot)$ is the sigmoid function and $\mathcal{N}(0,1)$ refers to the standard normal Gaussian distribution. $\tau_{min} = 20$ ms and $\tau_{step} = 105$ ms were used to constrain the parameter to range from 20 ms to 125 ms.

The schematic diagram of the model is shown in fig. 1a. All the models were implemented with TensorFlow 1.10.0 and trained on NVIDIA GPUs (RTX A4000).

Experiments

Dynamic contextual decision-making task. With the goal of elucidating the computational principles governing the seamless integration of diverse information streams in dynamic information processing, we developed a novel dynamic context decision-making task for our RNN models. In this task, we orthogonally manipulated bottom-up sensory signals as well as two distinct time-varying top-down instruction signals: task context and attention. This experimental design enabled us to independently investigate the temporal dynamics and circuit configurations involved in processing each signal and their subsequent integration. Specifically, we trained RNNs to perform variants of a delayed match-to-sample (DMS) task paired with an opposite anti-DMS task (fig. 1a,b). On each trial, two stimuli were presented sequentially, containing information about either one (fig. 1a) or two sensory modalities (fig. 1b; only one of which was contextually relevant in each trial). In the pro-DMS task, the agent's goal was to produce a +1 output when the two stimuli of the relevant modality matched, and a -1 when they did not. Conversely, the opposite responses were expected when an anti-DMS context was instructed. In the one-modality DMS task, a task cue signal representing which task to perform (pro-DMS vs. anti-DMS) was presented during the instruction period. In the two-modality task, the signal for which modality to attend to (attention cue) and which task to perform (task cue) was conveyed during the instruction period. Crucially, we manipulated the temporal dynamics of instructions, by presenting instructions early (before stimuli) or late (during the delay period in between two stimuli). Stimuli and instruction signals were presented for 250 ms each.

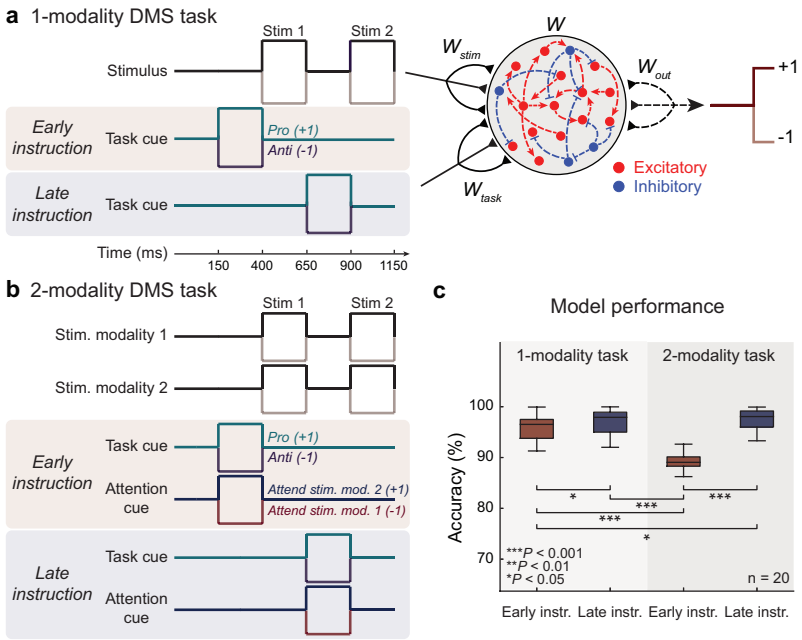

Fig. 1 | Delayed match-to-sample (DMS) tasks and model schematic. **a**) Schematic of a 1-modality DMS task with sequential stimuli separated by a delay interval. A task cue, indicating the stimulus-response mapping, is presented either before (*Early instruction*) or after stimulus 1 (*Late instruction*). The RNNs generate an output of +1 or -1 for matched and mismatched trials, respectively (*Pro*; and vice versa for *Anti*). **b**) Schematic of a 2-modality DMS task where each stimulus comprises two modalities. In addition to the task cue, an attention cue is presented on each trial, indicating the modality on which the RNNs need to perform the DMS task. The trial timing for both 1- and 2-modality DMS tasks is depicted in *a*). The task and attention cues are presented either before (*Early instruction*) or after stimulus 1 (*Late instruction*). **c**) Testing performance of the RNNs on the DMS tasks. The average accuracy of the trained RNNs is presented, with statistical significance computed using two-sided Wilcoxon rank-sum tests. Boxplot: central lines, median; bottom and top edges, lower and upper quartiles; whiskers, 1.5 × interquartile range; outliers are not plotted.

Training & testing protocol. Our model training was deemed successful if the following two criteria were satisfied within the first 70,000 epochs: 1) loss value (defined as the root mean squared error between the network output and target signals) < 7; and 2) task performance $> 95\%$ for the one-modality task and $> 85\%$ for the two-modality task. If the network did not meet the criteria within the first 70,000 epochs, the training was terminated. For each successfully trained RNN, we simulated 400 trials for the one-modality task and 1000 trials for the two-modality task, randomizing each trial to contain one possible combination of instruction order, task instruction, and stimulus identities. Using these criteria, we trained 20 RNNs for each task. Investigating the performance based on the timing of the top-down instruction signals revealed that the average task

accuracy was lower when the instruction was given before the first stimulus presentation for both tasks (fig. 1c).

Characterization of network motifs and circuit configurations

Decoding analysis. To characterize the stability of information representation in our RNN models, we performed a decoding analysis utilizing support vector machine (SVM) models. For each trained RNN, we obtained firing rate estimates of all the neurons across multiple trials. We then used the first half of the trials to train SVM models to decode task-related information. Subsequently, we tested each SVM on the left-out trials and computed the decoding accuracy at each time step.

Additionally, to determine whether RNNs preserved the geometry of stimulus coding across task conditions, we performed cross-condition generalization analyses, training and testing across time bins and across task conditions of interest[13]. We determined that top-down task signals, indicating pro-DMS vs. anti-DMS trials, were easily decodable from both the one-modality and two-modality models, immediately following the instruction presentation (fig. 2a-d). For both models, at the time of the second stimulus presentation, task signal decoding was stronger along the diagonal (i.e., training and testing at the time of second stimulus) than when training at the time of the first stimulus and testing cross-temporally at the second stimulus. This indicates that while task demands are represented throughout the trial, there is a dynamic shift in their representations in between stimulus presentation windows (as captured by the linear SVMs).

Furthermore, we set out to decode the top-down attention signal indicating which modality is relevant in each trial for the two-modality model. Once again, we were able to successfully decode these signals from neural populations immediately following the instruction period (fig. 2e-f). More importantly, we could also decode the identity of the attention signal during the first stimulus and delay periods for both attended (fig. 2g) and unattended (fig. 2h) modalities (for trials where the attention signal was given before the first stimulus). This indicates that both top-down attention and bottom-up stimulus signals are encoded by the network, and that the model is able to maintain bottom-up modality information even in the presence of top-down signals. We also measured SVM decoding performance for stimulus identity when training in early instruction trials and testing in late instruction trials, and vice versa. We found stable representation for stimulus identities in the one-modality models, as well as both sensory modalities in the two-modality model variants (Supplementary Figure 1).

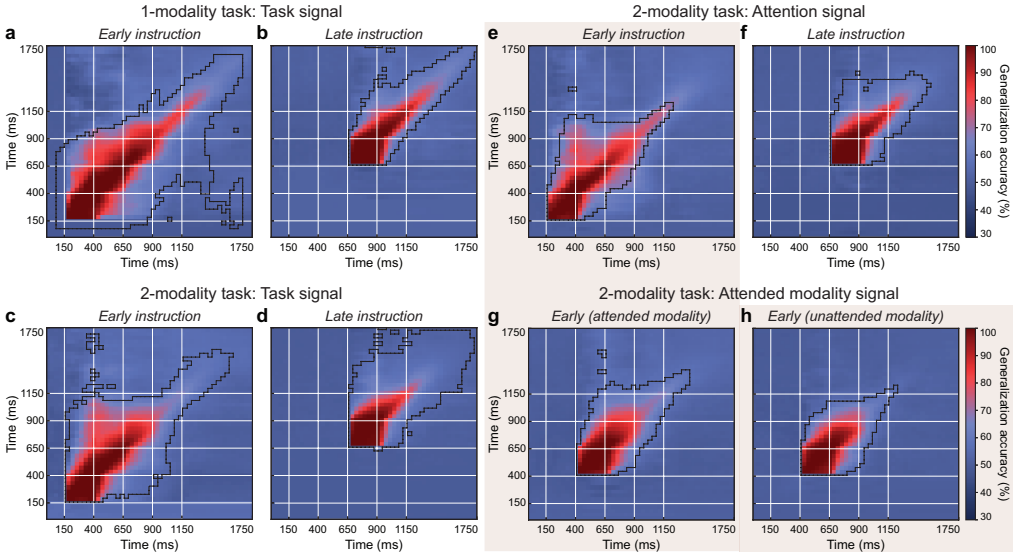

Fig. 2 | Temporal encoding of top-down signals during DMS tasks. Cross-temporal decodability of task and attention signals in the 1- and 2-modality DMS tasks is shown as the average generalization accuracy for each pair of training/testing time windows. Highlighted boundaries indicate significant decoding accuracies, $p < 1e-20$, binomial test, Bonferroni corrected. **a**) and **b**) Dynamic coding of the task signal ($Pro/Anti$) extending to the onset of the response period (1150 ms) is evident in both the *Early* and *Late instruction* conditions of the 1-modality task. **c**) and **d**) Similar patterns of dynamic codes for the task signal are observed for the 2-modality task, illustrating the robust encoding of the task identity. **e**) and **f**) Reliable decoding of the attention signal, indicating whether to attend to stimulus modality 1 or 2, can be observed over time in both the *Early* and *Late instruction* conditions. **g**) and **h**) In the *Early instruction* condition, the representation of the attention signal can be found during the stimulus 1 and delay interval, in the RNN activity corresponding to both the attended (**g**) and unattended stimulus modalities (**h**). White lines denote the reference event of each trial period (task/instruction cue, stimulus onsets, response).

State space analysis. To characterize how RNNs flexibly adapted to different task and attention demands, we performed a state space analysis, treating RNNs as a high-dimensional dynamical system. The goal of this analysis was to map how the energy landscape of the network changed as a function of inputs, providing a summarized account for the effect of task and attention demands over network dynamics. For this, we defined and minimized an auxiliary kinetic energy function $q(x, u) = \frac{1}{2}|F(x, u)|^2$, where $F(x, u) = \frac{dx}{dt}|_u$, utilizing the previously defined system dynamics from Equation 3, where x is the population state vector and u is the input to the network, containing stimulus, task, and modality cue information. Notably, $q(x, u) = 0$ if and only if the neural population state x is a fixed point, a point in which the velocity of the dynamic system is zero along every dimension [14, 15]. Along with fixed points, finding non-zero local minima of the

energy landscape, defined as slow points, is also useful, since both fixed points and slow points may be used to locally linearize the dynamic system and summarize its activity [14].

To identify slow points and visualize networks' energy landscape, we minimized $q(x, u)$ for all the possible values of u during the early instruction period, and demonstrated how top-down instructions reshape the activity of one example network prior to receiving bottom-up stimulus information. For the one-modality model, we tested the effect of instruction inputs in the pro-DMS, anti-DMS, or late instruction conditions. For the two-modality model, we tested u in each of the 4 possible combinations between pro/anti-DMS inputs and the two cued attentional modalities.

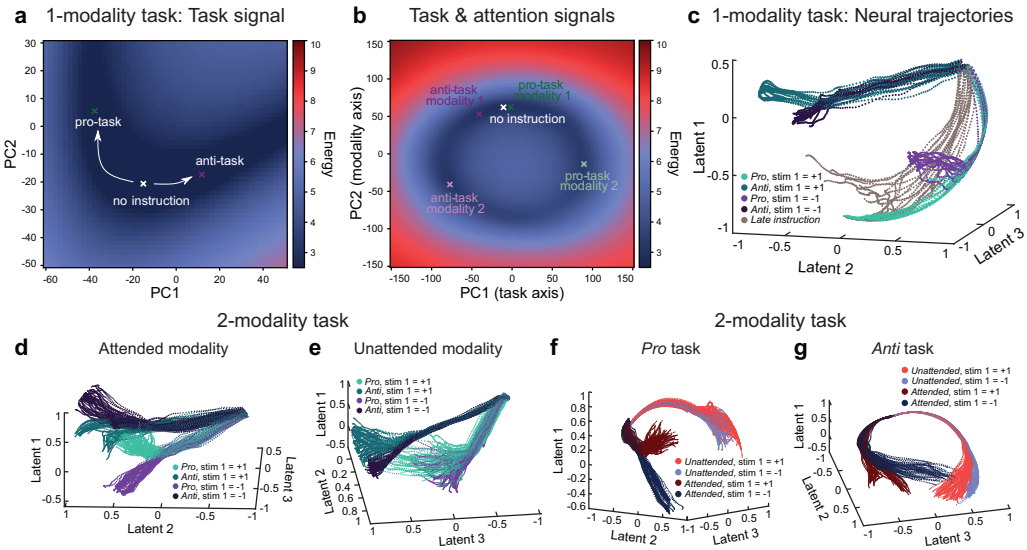

Fig. 3 | Task and attention representations in RNN state space. **a**) Heat map of kinetic energy in the one-modality RNN during the instruction period, when no task information is available. The middle cross indicates the local energy minimum for the no-task condition, while the left and right crosses indicate the new local energy minima for the pro-DMS and anti-DMS conditions, respectively. **b**) Same as **a**, for the two-modality RNN. Clockwise from the left-most point, minima indicate the following conditions: (anti-DMS and first modality attended), (anti-DMS and second modality attended), (pro-DMS and first modality attended), and (pro-DMS and second modality attended). **c**) Latent space one-modality RNN trajectories during instruction and first stimulus periods for all combinations of task instructions and stimulus identities. **d**) Same as **c**, for two-modality networks, highlighting the attended stimulus modality. **e**) Same as **c**, for two-modality networks, highlighting the unattended stimulus modality. **f**) Latent space two-modality RNN trajectories for pro-DMS trials, splitting trajectories by the identity of attended versus unattended cues. **g**) Same as **f**, for anti-DMS trials.

We performed minimization both in principal component space and in native space (with the *sklearn* module *optimize.minimize*), finding qualitatively similar results. For this analysis, we

defined principal components using the average activity of neurons in the early instruction period as features. We found that the one-modality models defined an inverted U-shape energy landscape, in which each branch contains one local minimum, for either DMS or anti-DMS inputs. Additionally, a third local minimum exists in the middle, for when the task instruction has not yet been presented to the network (fig. 3a and Supplementary Figure 2). Notably, each task's local minimum was roughly equidistant from the central local minimum. Interestingly, the example 2-modality network defined a ring-like energy landscape containing 4 distinct local minima for each combination of task instruction and attention cue (fig. 3b and Supplementary Figure 2).

Therefore, the top-down task input signals reshape the energy landscape of the network and nudge neural trajectories to a preferred path prior to stimulus presentation. Subsequently, the same stimulus inputs can lead to separate trajectories due to their distinct initial conditions. We confirmed this by selecting an example network and visualizing its latent network trajectories during early instruction and first stimulus periods, as obtained through the unsupervised manifold discovery method CEBRA [16]. The presence of task instructions distinguished trajectories, which further bifurcated upon receiving bottom-up sensory information about stimulus identity (fig. 3c).

We further used the CEBRA manifold representation to summarize the distinct effects of sensory-based (attention cue) and sensory-independent top-down information (task cue) over neural trajectories. In the two-modality task, the network trajectories bifurcated based on the task instruction (pro-DMS or anti-DMS) regardless of which modality was cued (fig. 3d,e). More specifically, the first stimulus identity (-1 or +1) for the cued modality were coded in distinct trajectories following the stimulus presentation (fig. 3d). On the other hand, the trajectories collapsed across the two stimulus identities for the unattended modality, even though the task coding was preserved (fig. 3e). We further confirmed this result by investigating whether attended versus unattended modalities were differentially represented in the latent space for pro-DMS trials versus anti-DMS trials (for both early and late instruction conditions; fig. 3f,g and Supplementary Figure 3, respectively). For both pro-DMS and anti-DMS trials, the latent trajectories split depending on the attention signal such that the attended trajectories further bifurcated based on the attended stimulus identities. However, the trajectories for the unattended modality did not separate based on the unattended stimulus identities. Taken together, these results highlight the differential utilization of top-down signals and provide compelling evidence that our model can asymmetrically employ distinct top-down signaling to optimize efficient coding of bottom-up sensory information.

Inhibitory-to-inhibitory connections carry top-down information

To better understand the circuit mechanisms required for flexible integration of the sensory signals and task-specific top-down information, we first identified neurons selective to the task cue signal (i.e., pro-DMS vs. anti-DMS) in the one-modality RNNs. Using the method described in the supplementary material, we discovered four distinct subgroups of neurons within each one-modality RNN: excitatory and inhibitory neurons tuned to the pro-DMS task cue signal, as well as excitatory and inhibitory neurons tuned to the anti-DMS task context. Interestingly, we observed that reducing the synaptic inputs (by reducing incoming synaptic weights by 50%) to the inhibitory neurons specific to the task context effectively eliminated the task cue signaling during the instruction window prior to the presentation of the first stimulus. For instance, decreasing the synaptic inputs to the inhibitory neurons biased toward the anti-DMS task in a one-modality RNN disrupted the anti-DMS task signaling. Consequently, the network exhibited a tendency to perform the pro-DMS task irrespective of the task context, as illustrated in (fig. 4a). By visualizing the neural dynamics of this "lesioned" network using CEBRA, we confirmed that the neural trajectories were no longer separated by the task cue signal during the instruction period (fig. 4b).

Motivated by the above observation, we systematically reduced synaptic inputs (by reducing incoming synaptic weights by 50%) to the anti-DMS preferring neurons in all the RNNs trained for the one-modality network model ($n = 20$ RNNs). This manipulation revealed that the largest decrease in model performance for the anti-DMS task occurred when inhibitory synaptic inputs to the anti-DMS preferring inhibitory neurons were decreased (indicated as I→I in fig. 4c). Additionally, reducing the inhibitory inputs to the excitatory neurons biased toward the anti-DMS task also resulted in a significant decrease in model performance (I→E in fig. 4c). Manipulating excitatory synaptic inputs did not lead to significant changes (E→I and E→E in fig. 4c). Similar results were observed when we lesioned neurons preferring the pro-DMS task context (see Supplementary Figure 4).

Performing the above analysis in the two-modality RNNs showed that disrupting the inhibitory input signaling to the inhibitory neurons specific to the anti-DMS task did not lead to a comparable drop in performance (fig. 4d). Furthermore, we found that the networks remained robust to manipulations of the synaptic inputs targeting the neurons selective for the attention signal. For instance, when we reduced the synaptic inputs to the neurons tuned to the first modality signal, we did not observe a complete loss of the attention signaling (fig. 4e).

The robustness of the two-modality networks to the above manipulations could be attributed

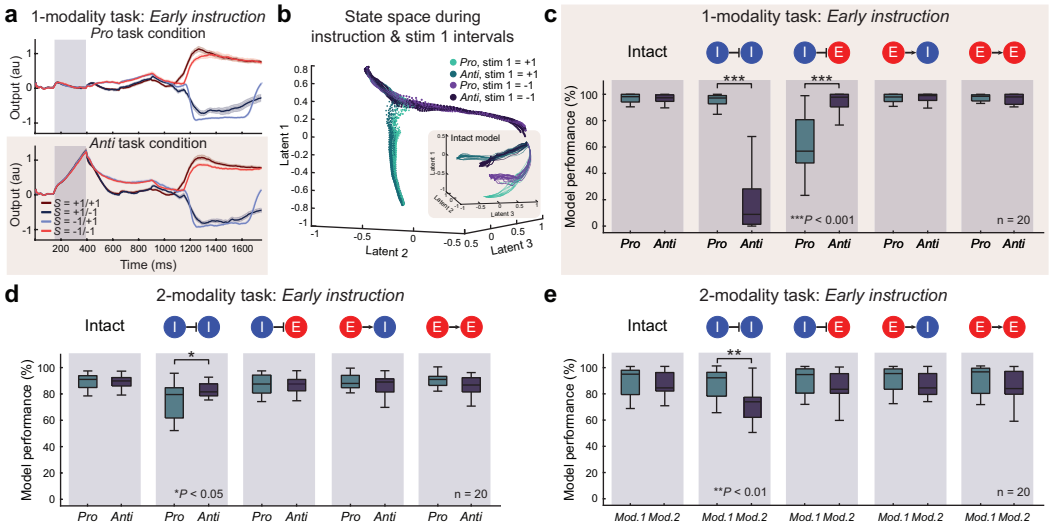

Fig. 4 | I→I connections encode top-down information. **a**) Reducing incoming inhibitory synaptic weights to inhibitory neurons selective to the anti-DMS cue by 50% in an example one-modality RNN led to the network performing the pro-DMS even when the anti-DMS cue was given (bottom). **b**) CEBRA neural trajectories of the lesioned model shown in **a** during the first instruction and stimulus periods. Inset, trajectories from the intact network (identical to fig. 3c). **c**) Performance of all 20 RNNs trained to perform the one-modality task when incoming synaptic weights (separated by excitatory and inhibitory weights) to anti-DMS preferring neurons (separated by excitatory and inhibitory) were reduced by 50%. **d**) Similar to **c**, for the two-modality RNNs. **e**) Similar to **d**, but when modality 1 attention cue selective neurons were lesioned. Statistical significance computed using the Wilcoxon signed rank test. Boxplot: central lines, median; bottom and top edges, lower and upper quartiles; whiskers, 1.5 × interquartile range; outliers are not plotted.

to the emergence of neurons that multiplex or encode multiple top-down factors (i.e., task and attention cues) simultaneously (Supplementary Figure 5). These neurons exhibit the capacity to integrate and represent multiple sources of top-down information, contributing to the network's ability to maintain stable performance despite perturbations in a subgroup of neurons.

Hierarchical organization of inhibitory-to-inhibitory feedback connections

In this section, we extended our RNN model to introduce an additional constraint to simulate a cortical hierarchy. In contrast to the previous configuration where all neurons in a network received input signals, we imposed a constraint restricting the input signals to a specific subpopulation within the network, effectively creating a distinct group of "sensory" neurons (fig. 5a). The network size (N) remained unchanged at 1000 neurons, but only 200 neurons received the input signals. Training this model on the one-modality task revealed that both "sensory" neurons and "non-

sensory" units encoded both bottom-up and top-down information (latent neural trajectories of the "sensory" units from an example model shown in fig. 5b).

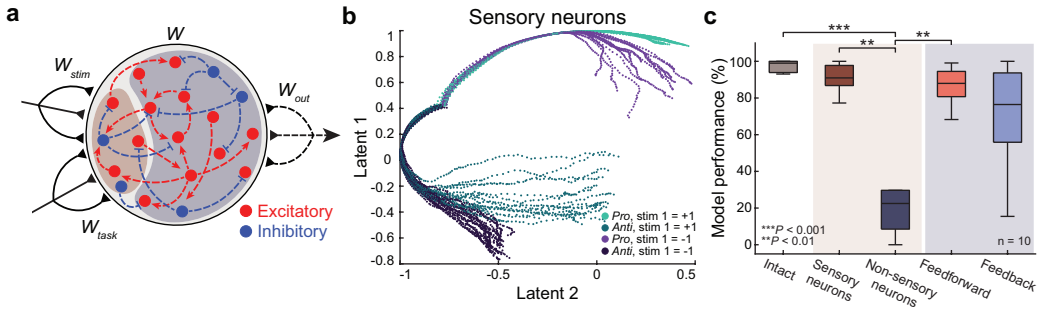

Fig. 5 | RNN model with input signaling constraints. **a**) Model schematic. The stimulus and task-related signals are only given to the first 200 units. **b**) CEBRA neural trajectories of the "sensory" neurons in an example RNN trained to perform the one-modality task. **c**) Anti-DMS task performance (across 10 RNNs) when I→I connections selective for the anti-DMS task signal were reduced by 50%. Statistical significance computed using Kruskal-Wallis test with Dunn's post hoc test. Boxplot: central lines, median; bottom and top edges, lower and upper quartiles; whiskers, 1.5 × interquartile range; outliers are not plotted.

We performed lesion studies on these networks, similar to the ones presented in the previous section. We found that selectively disrupting the inhibitory-to-inhibitory connections specific to the task cue within the non-sensory area had a pronounced effect on the model's performance (fig. 5c). Lesioning I→I signaling from the non-sensory area to the sensory area also resulted in a significant decrease in the task performance. Notably, disrupting the inhibitory-to-inhibitory connections within the "sensory" area did not lead to any impairment in task performance, suggesting that these synapses do not participate in stimulus encoding. Given our results from the previous section highlighting the importance of I→I synapses in encoding of the task context, the current findings in fig. 5c can be attributed to the higher abundance of I→I connections within the non-sensory area (which was modeled after experimental studies showing the increase in diverse inhibitory neuronal populations along the cortical hierarchy [17]).

Discussion

In this work, we proposed a framework that employs a biologically plausible RNN model and variants of a delayed match-to-sample (DMS) task to study how bottom-up (i.e., encoding sensory stimuli) and top-down (i.e., task instructions, attention) are integrated to facilitate flexible decision making. While previous works modeled flexible dynamic learning in biological [1, 18] and artificial [15, 19] agents, our work revealed the mechanisms through which an artificial neural network meets

such demands dynamically under relevant biological constraints. Specifically, we constrained the connectivity structure of our RNN model with Dale's principle and enforced heterogeneous synaptic timescales along with regionally specialized sensorimotor areas to model the neocortical hierarchy.

Using this model with important biological constraints, we demonstrated how our model dynamically coded signals containing sensory, instructional, and attentional information, and how this coding could be selectively disrupted by lesioning specific subsets of neurons, which revealed a privileged role for inhibitory projections in enabling instruction-dependent task performance. These results provide a substrate for future work in developing agents which can dynamically generalize their performance across different sensory environments, accommodating for fluctuations in top-down contextual signals. Additionally, our work provides a framework to generate testable hypotheses to further investigate the neural mechanisms of flexible and dynamic decision making in biological agents.

This work includes a number of limitations. While we enforced several elements of biological fidelity, future work can still be done to further approximate neural network structure to cortical hierarchical specialization, an approach which has been successful in the sensory domain with convolutional neural networks [20, 21]. Additionally, this mechanistic approach must be extended beyond the DMS paradigm to more complex, naturalistic tasks, involving high-dimensional state and decision spaces. Another limitation of our study is the biological plausibility of gradient-descent optimization. One way to address this is to compare our findings with RNNs trained using alternative methods, including non-gradient descent approaches. One notable alternative is the First-Order Reduced and Controlled Error (FORCE) learning algorithm, which has shown success in training rate-based and spiking RNNs [22, 23]. However, it's important to note that FORCE learning currently does not support training the synaptic decay time constant, making direct comparisons with our models challenging.

References

1. Mante, V., Sussillo, D., Shenoy, K. V. & Newsome, W. T. Context-dependent computation by recurrent dynamics in prefrontal cortex. *Nature* **503,** 78–84 (2013).

2. Song, H. F., Yang, G. R. & Wang, X.-J. Training Excitatory-Inhibitory Recurrent Neural Networks for Cognitive Tasks: A Simple and Flexible Framework. *PLOS Computational Biology* **12,** e1004792 (2016).

3. Miconi, T. Biologically plausible learning in recurrent neural networks reproduces neural dynamics observed during cognitive tasks. *Elife* **6,** e20899 (2017).

4. Yang, G. R., Joglekar, M. R., Song, H. F., Newsome, W. T. & Wang, X.-J. Task representations in neural networks trained to perform many cognitive tasks. *Nature Neuroscience* **22,** 297–306 (2019).

5. Werbos, P. J. Backpropagation through time: what it does and how to do it. *Proceedings of the IEEE* **78,** 1550–1560 (1990).

6. Kim, R., Li, Y. & Sejnowski, T. J. Simple framework for constructing functional spiking recurrent neural networks. *Proceedings of the national academy of sciences* **116,** 22811–22820 (2019).

7. Rungratsameetaweemana, N., Kim, R. & Sejnowski, T. J. Internal noise promotes heterogeneous synaptic dynamics important for working memory in recurrent neural networks. *bioRxiv.* eprint: `https://www.biorxiv.org/content/early/2022/10/18/2022.10.14.512301.full.pdf`. `https://www.biorxiv.org/content/early/2022/10/18/2022.10.14.512301` (2022).

8. Hendry, S. H., Schwark, H., Jones, E. & Yan, J. Numbers and proportions of GABA-immunoreactive neurons in different areas of monkey cerebral cortex. *Journal of Neuroscience* **7,** 1503–1519 (1987).

9. Sherwood, C. C., Raghanti, M. A., Stimpson, C. D., Bonar, C. J., de Sousa, A. A., Preuss, T. M. & Hof, P. R. Scaling of inhibitory interneurons in areas V1 and V2 of anthropoid primates as revealed by calcium-binding protein immunohistochemistry. *Brain, Behavior and Evolution* **69,** 176–195 (2007).

10. Alreja, A., Nemenman, I. & Rozell, C. J. Constrained brain volume in an efficient coding model explains the fraction of excitatory and inhibitory neurons in sensory cortices. *PLOS Computational Biology* **18,** e1009642 (2022).

11. Duarte, R., Seeholzer, A., Zilles, K. & Morrison, A. Synaptic patterning and the timescales of cortical dynamics. *Current Opinion in Neurobiology* **43,** 156–165 (2017).

12. Zador, A. M. & Dobrunz, L. E. Dynamic synapses in the cortex. *Neuron* **19,** 1–4 (1997).

13. Bernardi, S., Benna, M. K., Rigotti, M., Munuera, J., Fusi, S. & Salzman, C. D. The geometry of abstraction in the hippocampus and prefrontal cortex. *Cell* **183,** 954–967 (2020).

14. Sussillo, D. & Barak, O. Opening the black box: low-dimensional dynamics in high-dimensional recurrent neural networks. *Neural computation* **25,** 626–649 (2013).

15. Driscoll, L., Shenoy, K. & Sussillo, D. Flexible multitask computation in recurrent networks utilizes shared dynamical motifs. *bioRxiv,* 2022–08 (2022).

16. Schneider, S., Lee, J. H. & Mathis, M. W. Learnable latent embeddings for joint behavioural and neural analysis. *Nature,* 1–9 (2023).

17. Kim, Y., Yang, G. R., Pradhan, K., Venkataraju, K. U., Bota, M., García del Molino, L. C., Fitzgerald, G., Ram, K., He, M., Levine, J. M., Mitra, P., Huang, Z. J., Wang, X.-J. & Osten, P. Brain-wide Maps Reveal Stereotyped Cell-Type-Based Cortical Architecture and Subcortical Sexual Dimorphism. *Cell* **171,** 456–469.e22. ISSN: 0092-8674 (2017).

18. Yang, G. R., Cole, M. W. & Rajan, K. How to study the neural mechanisms of multiple tasks. *Current opinion in behavioral sciences* **29,** 134–143 (2019).

19. Yang, G. R., Joglekar, M. R., Song, H. F., Newsome, W. T. & Wang, X.-J. Task representations in neural networks trained to perform many cognitive tasks. *Nature neuroscience* **22,** 297–306 (2019).

20. Yamins, D. L. & DiCarlo, J. J. Using goal-driven deep learning models to understand sensory cortex. *Nature neuroscience* **19,** 356–365 (2016).

21. Nayebi, A., Bear, D., Kubilius, J., Kar, K., Ganguli, S., Sussillo, D., DiCarlo, J. J. & Yamins, D. L. Task-driven convolutional recurrent models of the visual system. *Advances in neural information processing systems* **31** (2018).

22. Sussillo, D. & Abbott, L. Generating Coherent Patterns of Activity from Chaotic Neural Networks. *Neuron* **63,** 544 –557 (2009).

23. Nicola, W. & Clopath, C. Supervised learning in spiking neural networks with FORCE training. *Nature Communications* **8,** 2208 (2017).

Acknowledgements

We gratefully acknowledge the support of the Swartz Foundation and Mission funding from the cooperative agreement under the United States Army Research Laboratory. Any opinions, findings, and conclusions or recommendations expressed in this material are those of the authors and do not necessarily reflect the views, policies, or endorsements, either expressed or implied, of the DEVCOM Army Research Laboratory or the U.S. Government.

Author contributions

All authors designed the study, performed the experiments, and wrote the paper.

Declaration of interests

The authors declare no competing interests.

Supplementary Figures

Supplementary Notes

Supplementary Table

	LIF	QIF
Membrane time constant (τ_m)	10 ms	10 ms
Absolute refractory period	2 ms	2 ms
Synaptic rise time (τ_r)	2 ms	2 ms
Constant bias current	-40 pA	0 pA
Spike threshold	-40 mV	30 mV
Spike reset voltage	-65 mV	-65 mV

Supplementary Table 1 | Parameter values used to construct LIF and QIF networks.